Monatsh Chem (2010) 141:847–858
DOI 10.1007/s00706-010-0345-x

ORIGINAL PAPER

Red electrophosphorescent platinum(II) quinolinolate complexes

Fabian Niedermair · Roman Trattnig · Kurt Mereiter · Martin Schmuck · Stefan Sax · Emil J. W. List · Christian Slugovc

Received: 22 January 2010 / Accepted: 9 June 2010 / Published online: 30 July 2010

Abstract Luminescent organoplatinum complexes featuring 8-quinolinolates as chelating ligands have been synthesized and characterized. Substitution of the quinolinolate ligand has been achieved in the 5 position, where benzoyl substituents were introduced by reacting 8-hydroxyquinoline and the corresponding benzoyl chloride in a Friedel–Crafts acylation. The resulting complexes, κ^2(N,C^2)-(2-(4-*tert*-butylphenyl)pyridine)-κ^2(N,O)-(5-(4-*tert*-butylphenyl)(8-quinolinolato-5-yl)methanone)platinum(II) and κ^2(N,C^2)-(3-hexyloxy-2-phenylpyridine)-κ^2(N,O)-((8-quinolinolato-5-yl)phenylmethanone)platinum(II), have been investigated by nuclear magnetic resonance and infrared spectroscopy, matrix-assisted laser desorption ionization time-of-flight mass spectrometry, X-ray analysis, thermal analysis, cyclic voltammetry, UV–vis absorption spectroscopy, and luminescence measurements in solution and in the solid state. The solid-state structures of the complexes were found to be dominated by π–π intermolecular interactions. Organic light-emitting devices based on the complexes and a matching host material gave red to near-infrared electroluminescence with low-onset voltages (4–5 V) and continuous wave luminance intensities exceeding 500 cd/m^2.

Keywords Organometallic compound · Material science · Organic light-emitting device · Phosphorescence · X-ray structure determination

F. Niedermair · M. Schmuck · C. Slugovc (✉)
Institute for Chemistry and Technology of Materials (ICTM), Graz University of Technology, Stremayrgasse 16, 8010 Graz, Austria
e-mail: slugovc@tugraz.at

R. Trattnig · S. Sax · E. J. W. List
Institute of Solid State Physics, Graz University of Technology, Petersgasse 16, 8010 Graz, Austria

R. Trattnig · S. Sax · E. J. W. List
NanoTecCenter Weiz Forschungsgesellschaft mbH, Franz-Pichler Strasse 32, 8160 Weiz, Austria

K. Mereiter
Institute of Chemical Technologies and Analytics, Vienna University of Technology, Getreidemarkt 9/164, 1060 Vienna, Austria

Introduction

Phosphorescent platinum(II) complexes have attracted great attention because of their applications in various fields such as chemical sensors [1–7], organic light-emitting devices (OLEDs) [8, 9], and photovoltaics [10]. In general, phosphorescent transition-metal complexes are promising candidates for use as emitters in OLEDs, as their strong spin-orbital coupling induces efficient intersystem crossing from the singlet to the triplet excited state. As a result, both singlet and triplet excitons can be used, which theoretically leads to internal quantum efficiencies of 100% [11]. Luminescence quantum yields of the complexes are significantly affected by the accessibility of the platinum-centered excited state through the population of the $d_{x^2-y^2}$ and the d_{z^2} orbitals, which opens up efficient nonradiative decay paths [6, 7, 12–17]. Increasing the energy of the *d*–*d* state by using ligands that impose a strong ligand field, such as cyclometalating ligands, is a way to overcome this drawback. A second strategy aimed at enabling efficient emission of Pt(II) complexes is to provide a low-lying ligand-centered emitting excited state that is not be quenched by the *d*–*d* state [18]. Nevertheless, quantum yields of neutral platinum(II) complexes in the solid state are low [19], and it is necessary to embed them into a suitable host material when applying them in phosphorescent devices.

The crucial issue in host material selection is to appropriately adjust the host's triplet energy level with respect to the triplet energy level of the emitting guest [20]. The triplet energy level of the latter must be lower than that of the host material, otherwise back transfer of triplet energy from the guest to the host could take place [21]. Excitation transfer from the host material to the metal–organic center in electrophosphorescent LEDs can occur by various mechanisms, including Förster and/or Dexter energy transfer [22]. In addition, temperature-activated migration of excitons towards the guest [23] as well as the direct sequential trapping of both electrons and holes on the phosphorescent guest can play a role [24].

Another issue relating to the applicability of electrophosphorescent dyes in OLEDs is their stability (chemical and thermal). It has been shown that commonly used acetylacetonate (acac)-bearing complexes are unstable in the presence of poly(3,4-ethylenedioxythiophene):poly(styrenesulfonate) (PEDOT:PSS) in electroluminescent devices [24, 25], and that they tend to decompose at temperatures at which vacuum deposition usually occurs [26]. For this reason, we evaluated 8-quinolinolate derivatives (Q) as co-ligands in organoboron [27], cyclometalated iridium(III), and platinum(II) complexes [28–32]. Q ligands are isoelectronic with acac-type ligands, but—and in contrast to typical ancillary ligands like acac—8-quinolinolate complexes often emit from a Q-based excited state (e.g., the most prominent example $Al(Q)_3$) [33]. In platinum chemistry, homoleptic $Pt(Q)_2$ complexes are known to emit from a triplet intraligand charge transfer (^{3}ILCT) [34–36], and two recent reports on cyclometalated Pt(II) complexes with 8-quinolinolates as the co-ligands precede this work, and give an impression of the scope of this particular class of complexes for singlet oxygen generation [37] and as near-infrared emitting materials in OLEDs [19].

Herein, the synthesis and characterization of two electrophosphorescent heteroleptic Pt(II) complexes bearing modified 2-phenylpyridine as the cyclometalating ligands and two differently substituted (8-hydroxyquinolin-5-yl)methanone derivatives as the non-spectator ligands are reported. Emphasis is placed on investigating the role of the substituents on the physical and photophysical properties of the corresponding complexes.

Results and discussion

Synthesis

The title compounds **3a** and **3b** were prepared by the reaction of the precursor materials κ^2(N,C^2)-(2-(4-*tert*-butylphenyl)pyridine)-κ^1(N)-(2-(4-*tert*-butylphenyl)pyridine)-chloroplatinum(II) (**1a**) and κ^2(N,C^2)-(3-hexyloxy-2-phenylpyridine)-κ^1(N)-(3-hexyloxy-2-phenylpyridine)chloroplatinum(II) (**1b**) [38] with (4-*tert*-butylphenyl)-(8-hydroxyquinolin-5-yl)methanone (**2a**) and (8-hydroxyquinolin-5-yl)phenylmethanone (**2b**) [39] in the presence of K_2CO_3 as the base (Scheme 1).

The reactants were dissolved in a mixture of CH_2Cl_2/EtOH = 1/1 (v/v) and stirred under an inert atmosphere of Ar for 24 h at room temperature. Purification was accomplished by flash chromatography using neutral Al_2O_3 ($R_f = 0.35$ for **3a** and $R_f = 0.88$ for **3b** in CH_2Cl_2 on neutral Al_2O_3). Washing of the solid with *n*-pentane was used as a further purification step, yielding 60% (**3a**) and 76% (**3b**) of the analytically pure compounds. Complexes

Scheme 1

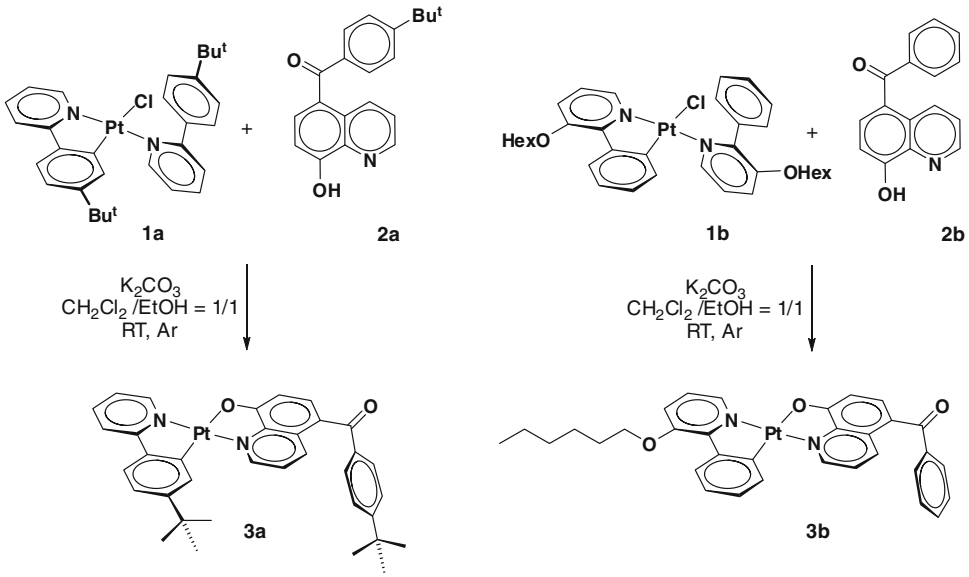

3a and **3b** are soluble in $CHCl_3$ and acetone, but are insoluble in diethyl ether and *n*-pentane. **3a** is far less soluble than **3b**, meaning that the two *tert*-butyl groups of **3a** do not exert a similar beneficial influence on the compound's solubility to the hexyloxy group present in **3b**. Attachment of the hexyloxy group at position 3 of the pyridine core has already been shown to increase the solubilities of similar complexes bearing dihydridobis (pyrazolyl)borate as the second co-ligand [38]. Complexes **3a** and **3b** are air stable in solution and in the solid state and were characterized by ^{1}H NMR, $^{13}C\{^{1}H\}$ NMR, infrared spectroscopy, and high-resolution matrix-assisted laser desorption ionization time-of-flight mass spectrometry (MALDI-TOF-MS). The ^{1}H NMR spectra of **3a** and **3b** revealed the presence of a single diastereomer [31, 32]. No special features aside from this were observed, and the corresponding data are given in the "Experimental" section. Fourier transform infrared measurements of complexes **3a** and **3b** exhibited characteristic signals for the PhCO stretch vibration at 1,634 and 1,629 cm^{-1}, respectively. The strongest peak in the spectra of **3a** and **3b**, which occurred at 1,503 cm^{-1}, was attributed to an asymmetric C–C vibration of the phenolic part of the Q ligand.

X-ray crystallography

The crystal structures of complexes **3a** and **3b** were studied by X-ray diffraction in order to learn about their geometries, packing, and mutual interactions in the solid state. Complex **3a** formed an unsolvated solid state form, whereas complex **3b** crystallized as two different solvates with CH_2Cl_2, namely **3b**·1/2CH_2Cl_2, and **3b**·3/2CH_2Cl_2. Details of the crystal structure determinations are reported in the "Experimental" section. The molecular structures of the complexes in these crystal forms are shown in Figs. 1 and 2, and selected geometric parameters are given in Table 1. In all three solids, platinum has a distorted square-planar coordination with very similar bond lengths and bond angles, which correspond well with two previously

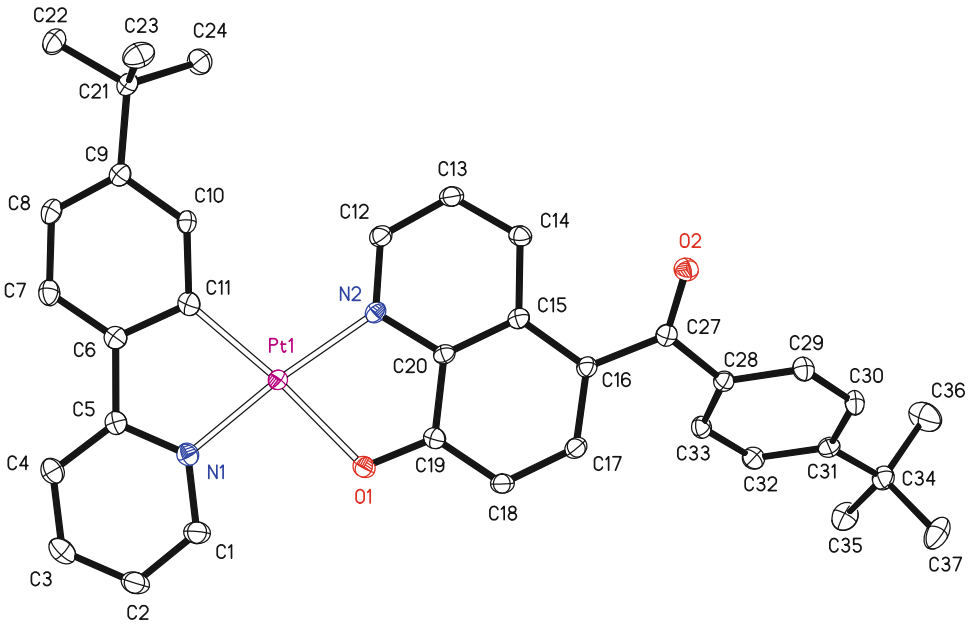

Fig. 1 Structural view of the Pt complex in **3a**. H-atoms are omitted for clarity

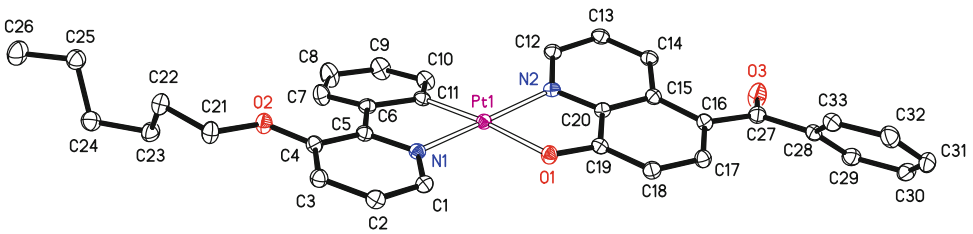

Fig. 2 Structural view of the Pt complex in **3b**·3/2CH_2Cl_2, demonstrating the nonplanarity of the the Pt(PhPy)(8-OH-quin) moiety due to steric interference between the hydrogen atoms (not shown) of C10 and C12. Note also the kinked hexyloxy side chain, which is all-*trans* and stretched in the crystal structure of **3b**·1/2CH_2Cl_2

Table 1 Selected geometric parameters (Å, °) for **3a**, **3b**·1/2CH_2Cl_2, and **3b**·3/2CH_2Cl_2

	3a	**3b**·1/2CH_2Cl_2	**3b**·3/2CH_2Cl_2
Pt1–N1	1.997 (2)	1.992 (2)	1.998 (2)
Pt1–C11	1.986 (2)	1.992 (2)	1.979 (2)
Pt1–N2	2.024 (2)	2.037 (2)	2.020 (2)
Pt1–O1	2.095 (2)	2.093 (2)	2.100 (2)
N1–Pt1–C11	80.7 (1)	80.3 (1)	80.3 (1)
C11–Pt1–N2	104.3 (1)	106.2 (1)	104.0 (1)
N2–Pt1–O1	80.4 (1)	80.0 (1)	79.9 (1)
O1–Pt1–N2	94.7 (1)	93.6 (1)	96.1 (1)
Pt(PhPy)(8-OH-quin)[a]	0.160	0.137	0.278
$PtCN_2O$ square[a]	0.037	0.026	0.063
PhPy ligand[a]	0.067	0.095	0.113
8-OH-quinolinate[a]	0.038	0.042	0.055
∠ PhPy/(8-OH-quin)[b]	9.12 (7)	5.28 (7)	13.92 (5)
C10 out-of-plane[c]	0.398 (2)	−0.317 (2)	0.374 (2)
C12 out-of-plane[c]	−0.263 (2)	0.249 (2)	−0.536 (2)
PhPy distortion[d]	0.49	0.58	0.57

[a] RMS deviations (Å) of the corresponding non-hydrogen atoms from a common least-squares plane through them

[b] Angle between the least squares plane through the phenylpyridine and the 8-hydroxyquinoline ligand

[c] Deviation (Å) of the corresponding carbon atoms form the least-squares plane through Pt(PhPy)(8-OH-quin)

[d] Difference between the distances C4–C7 and N1–C11, showing the in-plane bending of the PhPy ligand caused by chelation

reported structures [28, 37]. Significant in-plane bending of the phenylpyridine ligand upon chelation can be noted in Figs. 1 and 2, which causes the intramolecular 1–4 distances N1–C11 and C4–C7 to differ by 0.5–0.6 Å (Table 1). With respect to their Pt(PhPy)(8-OH-quin) moieties, the complexes are approximately planar, but deviate very significantly from common least-squares planes because of the steric interference between the C–H groups of C10 and C12 (H–H contact distances of about 1.95 Å; deviations of the two carbon atoms from the complex mean planes of 0.25–0.55 Å in mutually opposite directions). This steric interference leads to interplanar angles between the PhPy and the 8-hydroxyquinoline ligand of 5.3° to 13.9°. The terminal benzoyl groups in all three solids are strongly inclined to their respective 8-hydroxyquinoline groups, which is also due to steric congestion. Despite the nonplanar shapes of the complexes, all three solids exhibit layered arrangements of their complexes in three-dimensional space, with significant π–π stacking interactions perpendicular to layers, as shown for **3b**·1/2CH_2Cl_2 (Fig. 3). In terms of crystallography, the orientation of the layers in the triclinic lattices varies widely, namely parallel to (1¯31) in **3a**, parallel to (2¯30) in **3b**·1/2CH_2Cl_2, and parallel to (1¯11) in **3b**·3/2CH_2Cl_2. The

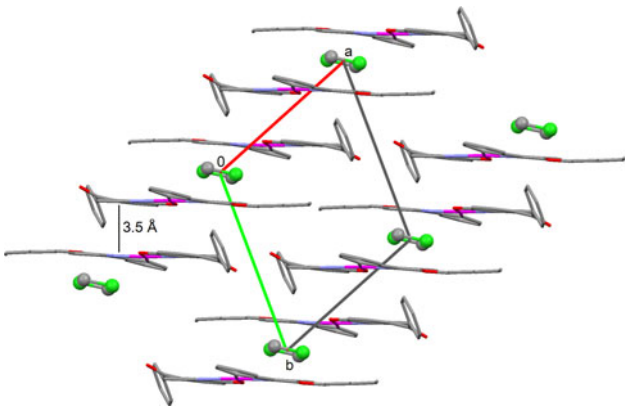

Fig. 3 Packing diagram of **3b**·1/2CH_2Cl_2 in stick representation viewing down the *c*-axis, showing the layered arrangement of the Pt complexes parallel to (230). CH_2Cl_2 molecules are shown in ball-and-stick representation

π–π stacking distances the PhPy ligands, which are predominately superimposed, are approximately in the range 3.3–3.5 Å. Pt–Pt interactions are not present in all three solids (all Pt–Pt distances are larger than 4.4 Å). It is interesting to note that complex **3b** forms two different crystalline solvates with CH_2Cl_2, one with 0.5 and one with 1.5 solvent molecules per Pt complex. Whereas **3b**·1/2CH_2Cl_2 exhibits an all-*trans*-configured hexyloxy chain similar to the complex described by Kappaun et al. [28], the same moiety in **3b**·3/2CH_2Cl_2 is kinked and shows two *gauche*-configured links (O2–C21–C22–C23 = 64°, C22–C23–C24–C25 = 60°).

Stability issues

The thermal stabilities of **3a** and **3b** were evaluated by heat flux DSC/TGA measurements performed under a nitrogen atmosphere. Complexes **3a** and **3b** gave distinct melting peaks at 278 and 230 °C, respectively. The temperature at a weight loss of 5% was used as an indicator of the thermal stabilities of the compounds. Measurements revealed a weight loss of 5% at 281 °C for **3a** and at 308 °C for **3b** (Fig. 4). Results show that both compounds are sufficiently stable to be able to use them as emitter materials in OLEDs [26, 40].

At 408 °C, a weight loss of ~52% was noted for **3a**, which indicates decomposition by "decoordination" of the (4-*tert*-butylphenyl)pyridine ligand together with the splitting off of the 4-*tert*-butylbenzoyl moiety (theoretical weight loss: 52%) (Fig. 4). The corresponding weight loss of ~52% for complex **3b** occurs at 403 °C, and is characterized by the decoordination of the 3-hexyloxy-2-phenypyridine ligand as well as the splitting off of the benzoyl moiety (theoretical weight loss: 52%) (Fig. 4).

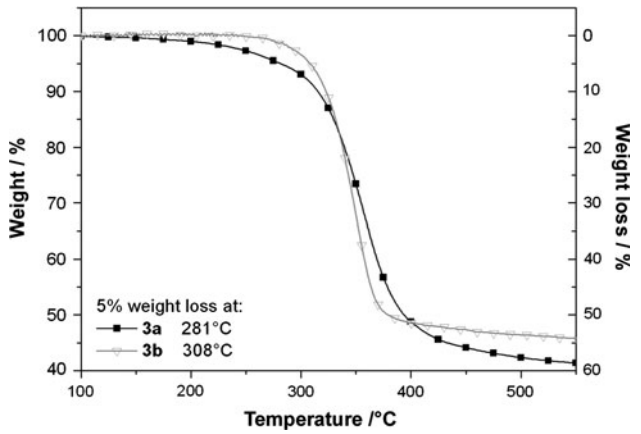

Fig. 4 TGA thermograms of compounds **3a** and **3b**

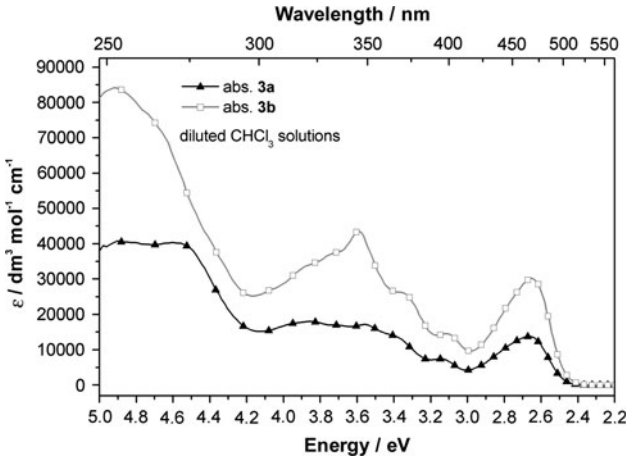

Fig. 5 Absorption spectra of **3a** ([**3a**] = 1.1 × 10^{-5} M) and **3b** ([**3b**] = 1.5 × 10^{-5} M) measured in $CHCl_3$ solution at room temperature

Another crucial parameter for applications in electroluminescent devices is the stability of the phosphorescent chromophores in the presence of acidic layers [25]. Sensitivity to trifluoroacetic acid (TFA) is a good indicator of this particular stability. Accordingly, ^{1}H NMR experiments monitoring the stability of the complexes in $CDCl_3$ containing 20 mm^3 $TFA_{conc.}$ at room temperature were performed [28–30]. **3a** and **3b** showed no decomposition over an observation period of 24 h.

Electronic absorption spectroscopy

The absorption spectra of complexes **3a** and **3b**, measured in diluted solutions of $CHCl_3$ at room temperature under ambient conditions, show a significant absorption band in the visible region. The lowest-energy absorption band is centered around 460–470 nm (Table 2; Fig. 5), with extinction coefficients (ε) of 13,800 for **3a** to 30,200 cm^{-1} M^{-1} for **3b**, and can be assigned to the ILCT transition of the Q chromophore [28, 37, 41]. Transitions associated with the C^N and [Pt(C^N)] chromophores were observed in the range 252–297 nm and 345–414 nm, respectively [37, 42, 43].

Luminescence spectroscopy

Compounds **3a** and **3b** in $CHCl_3$ solutions under ambient conditions emitted with emission maxima at 641 and 633 nm, respectively (Fig. 6). Degassed solutions of complexes **3a** and **3b** showed enhanced emission intensities, indicating the usual quenching of luminescence by oxygen. Quantum yields (Φ) of compounds **3a** and **3b** were measured in degassed $CHCl_3$. 4-Dicyanomethylene-2-methyl-6-(4-(dimethylamino)styryl)-4H-pyran (DCM) was used as the standard [44]. Quantum yields of 3.2 ± 0.9 for complex **3a** and 2.0 ± 0.9 for complex **3b** were

Table 2 Absorption and emission properties of the platinum(II) complexes **3a** and **3b** at room temperature

Complex	Abs, λ^a_{max} λ (nm) (ε [10^{-3} cm^{-1} M^{-1}])	Emission λ_{max} (nm)	τ^b_{Air} (μs)	τ^b_{N2} (μs)	τ_{77K} [c] (μs)	Φ^d (%)
3a	253 (40.8), 348 (17.1),	640[a]	2.0	12	21 ± 5	3.2 ± 0.9
	364 (14.2), 394 (7.4),	580[c]	(5.0)	(10)		(4 ± 3)[b]
	464 (13.8)	629[e]				
3b	252 (84.2), 345 (43.6),	633[a]	2.0	19	16 ± 5	2.0 ± 0.9
	371 (26.0), 398 (14.5),	583[c]	(4.0)	(18)		(3 ± 2)
	467 (30.2)	633[e]				

[a] $CHCl_3$ solutions, c = 4–15 × 10^{-6} M, room temperature

[b] Apparent lifetimes measured at a modulation frequency of 5.5 kHz in $CHCl_3$, c = 2 × 10^{-5} M, in parentheses: c = 3–4 × 10^{-6} M

[c] Emission at 77 K in CH_2Cl_2, c = 1–4 × 10^{-4} M

[d] Quantum yield, c = 3–4 × 10^{-6} M, in parentheses: c = 8–9 × 10^{-7} M, room temperature

[e] Thin-film emission maximum of a drop-cast film on glass (2 wt% complex in PMMA)

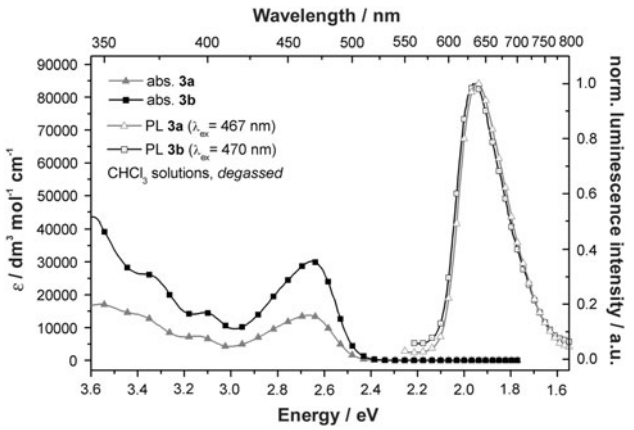

Fig. 6 Absorption spectra of **3a** ([**3a**] = 1.1×10^{-5} M) and **3b** ([**3b**] = 1.5×10^{-5} M) and emission spectra (degassed) of **3a** ([**3a**] = 3.8×10^{-6} M) and **3b** ([**3b**] = 5.2×10^{-6} M) measured in $CHCl_3$ solution at room temperature

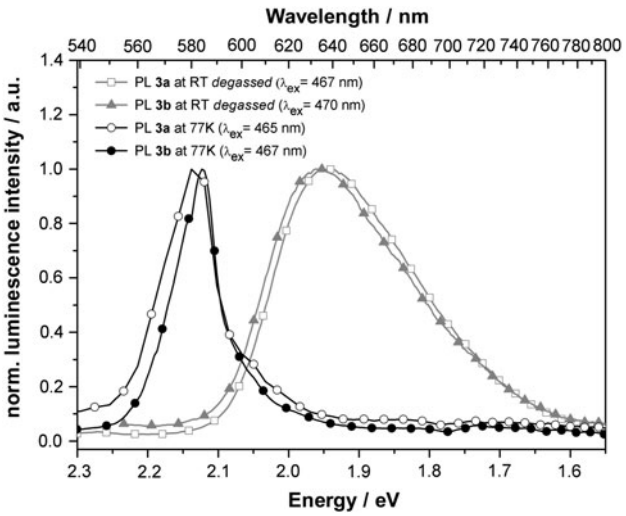

Fig. 7 Emission spectra of **3a** and **3b** measured in $CHCl_3$ at room temperature ([**3a**] = 3.8×10^{-6} M, $\lambda_{ex} = 467$ nm; [**3b**] = 5.2×10^{-6} M, $\lambda_{ex} = 470$ nm) and at 77 K ([**3a**] = 1.3×10^{-4} M, $\lambda_{ex} = 465$ nm; [**3b**] = 4.1×10^{-4} M, $\lambda_{ex} = 467$ nm)

determined. In contrast to similar quinolinolate complexes [31, 32], only a marginal concentration dependence of the quantum yield was observed (Table 2). This result may be best explained by a decreased tendency of the complexes under investigation to form aggregates in solution compared to their unsubstituted counterparts [31, 32]. Anyway, attachment of the bulky substituents in **3a** and **3b** opens up additional nonradiative relaxation pathways, resulting in rather poor quantum yields in solution.

Quenching by oxygen was characterized by measuring the luminescence lifetime (τ) in aerated and degassed solutions using a frequency-based method [45]. Apparent lifetimes of **3a** and **3b** in degassed solutions ranged from 10 to 19 μs. Values of τ showed a negligible dependence on the concentration of the complex solution (Table 2), which suggests that nonluminescent aggregates were formed at higher concentrations and, as discussed before, accounted for the lower quantum yields at higher concentrations.

Complexes **3a** and **3b** show relatively large rigidochromic blue shifts of 61 and 50 nm, respectively, on cooling the solution sample to 77 K (Fig. 7). This effect arises from variations in the dipolar interactions between the excited molecule and the solvent dipoles of the surrounding medium [46]. In the work of Fernández et al. [47], rigidochromic shifts in diluted CH_2Cl_2 solutions (298 vs. 77 K) in the range 20–30 nm were reported for anionic cyclometalated bis(alkynyl)(benzo[*h*]quinolinate)platinate(II) species. Thin-film emission spectra of complexes **3a** and **3b** (2 wt% complex in PMMA) revealed emission maxima of 629 nm for **3a** and 633 nm for **3b**, respectively.

Electrochemical measurements

Cyclic voltammetry was applied to estimate the energy levels of the highest occupied molecular orbital (HOMO) and the lowest unoccupied molecular orbital (LUMO). With some restrictions, the reduction and oxidation onsets of the CV peaks can be used to estimate the electron affinity (EA ≈ LUMO energy) and the ionization potential (IP ≈ HOMO energy) [48]. The first oxidation wave (even for irreversible oxidation waves) usually corresponds to the removal of an electron from the HOMO, and formally involves oxidation of Pt(II) to Pt(III) [49]. Assuming that the absolute level of the ferrocene/ferrocenium redox pair is 4.8 eV below the vacuum level gives a LUMO energy of −2.76 eV for both complexes. For **3a** and **3b**, the HOMO energies were found to be −4.73 and −4.69 eV, respectively (Table 3).

Electroluminescent properties

To determine the electroluminescent properties of **3a** and **3b**, OLEDs were fabricated on indium tin oxide-coated (ITO) glass substrates (spin-coated from THF solutions) in a device configuration of ITO/PEDOT:PSS/host material:platinum(II) complex (**3a** or **3b**)/cathode material under an inert atmosphere of argon in a glove box. For complexes **3a** and **3b**, the host material poly[(9,9-dioctylfluorenyl-2,7-diyl)-co-(*N*,*N*′-diphenyl)-[*N*,*N*′-bis(*p*-butylphenyl)]-1,4-diaminobenzene] (ADS232GE) was used (Fig. 8). Different cathode materials were applied to the corresponding OLEDs: while Ca/Al and CsF/Al were chosen in the case of **3b**, devices containing **3a** were only fabricated with a CsF/Al cathode layer. The emission wavelength of the chosen host material ($\lambda_{max} = 452$ nm) is in good accordance with the absorption peaks of **3a** and **3b** at 464 and 467 nm, respectively.

Table 3 Estimated HOMO/LUMO energies of **3a** and **3b**, as measured by cyclic voltammetry

Complex	Onset (V)	Reduction onset (V)	HOMO (eV)	LUMO (eV)	E_g (eV)
3a	−0.07	−2.04	−4.73	−2.76	−1.97
3b	−0.11	−2.04	−4.69	−2.76	−1.93

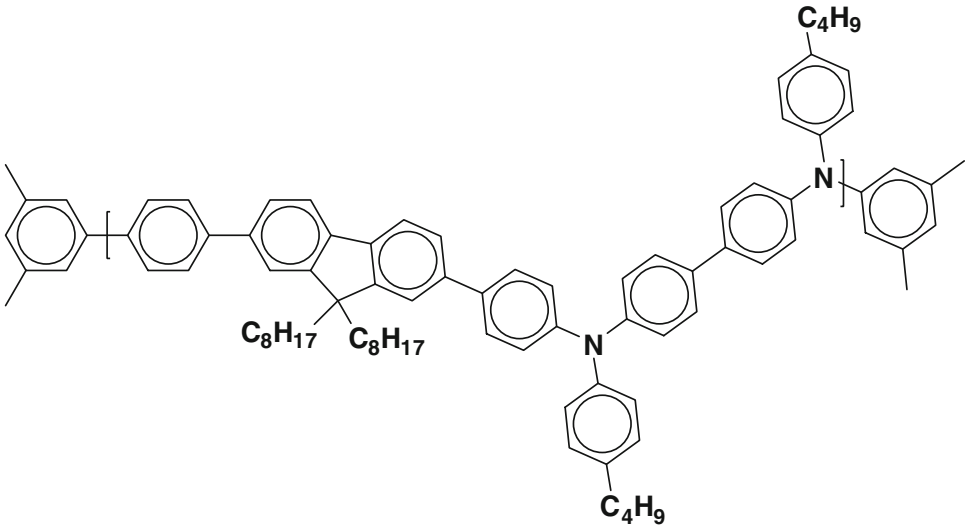

Fig. 8 The host material poly[(9,9-dioctylfluorenyl-2,7-diyl)-co-(*N*,*N*′-diphenyl)-[*N*,*N*′-bis(*p*-butylphenyl)]-1,4-diaminobenzene] (ADS232GE, $\lambda_{max,abs} = 380$ nm, $\lambda_{max,em} = 452$ nm; redrawn according to American Dye Source, Inc.)

Devices with different complex loadings of **3b** were fabricated using Ca/Al as cathode material. Significant concentration quenching was observed for this class of materials; for example, a maximum luminance of 110 cd/m^2 at 10 V was obtained for devices containing 3 wt% of **3b**, whereas devices prepared with 5 or 10 wt% of **3b** gave luminance values of around 75 and 40 cd/m^2, respectively, at the same voltage. Devices fabricated with complex **3b** and CsF/Al as cathode material showed higher luminance values at the corresponding voltage than devices consisting of Ca/Al cathodes. This effect is mainly related to a reduction of the injection barrier for electrons due to the lower work function of CsF, which can therefore enhance exciton formation [50, 51]. The luminance values were around 500 cd/m^2 (for 3 wt% of **3b**), 300 cd/m^2 (for 5 wt% of **3b**), and 100 cd/m^2 (for 10 wt% of **3b**) at 9 V (Fig. 9). Similar concentration quenching to that seen for the Ca/Al devices was observed, and again the blue host emission at 458 nm could be significantly reduced by using a higher guest dye concentration. As a result, pure red electroluminescence at 625 nm with a shoulder at around 660 nm was observed with onset voltages ranging from 4 to 5 V (Figs. 9, 10, 11). The occurrence of the mentioned shoulder points to exciplex formation between the host material and the complexes under investigation. Anyway, a considerable improvement compared to devices presented recently was achieved [19, 52].

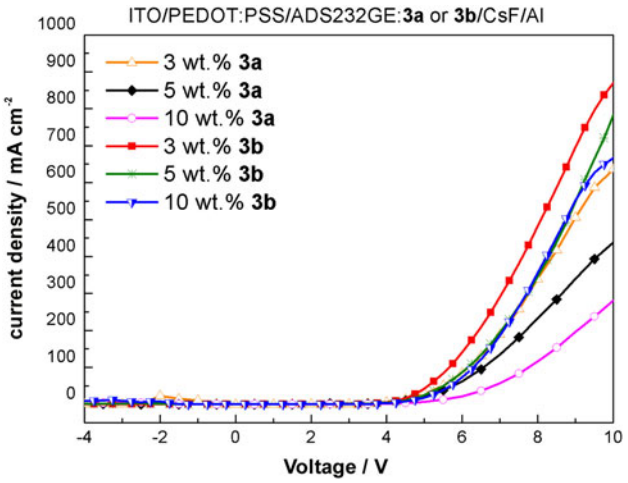

Fig. 9 Current density versus voltage characteristics of devices containing various amounts of **3a** or **3b** blended with ADS232GE as an active layer (device configuration: ITO/PEDOT:PSS/ADS232GE: **3a** or **3b**/CsF/Al)

Since no significant influence of the chosen cathode materials on the EL emission spectra of devices containing **3b** was found, further devices comprising **3a** consisted exclusively of CsF/Al cathodes. Corresponding devices containing 3 wt% of **3a** showed pure red electroluminescence at 627 nm with a shoulder at about 670 nm with onset voltages of around 4 V (Fig. 9, 11). Quenching of electrophosphorescence due to a higher platinum complex

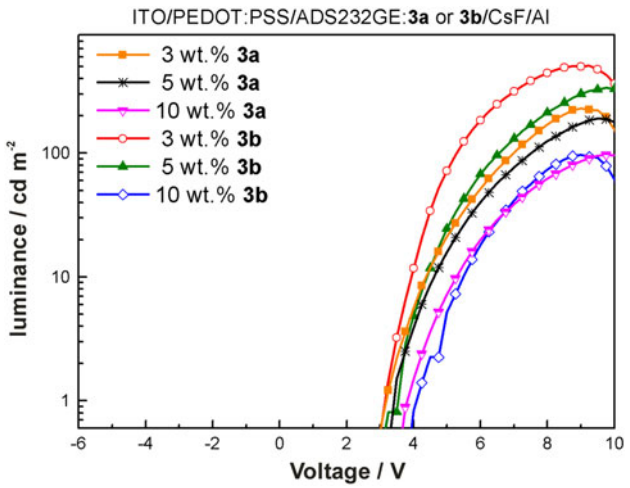

Fig. 10 Luminance versus voltage characteristics of devices containing various amounts of **3a** or **3b** blended with ADS232GE as an active layer (device configuration: ITO/PEDOT:PSS/ADS232GE: **3a** or **3b**/CsF/Al)

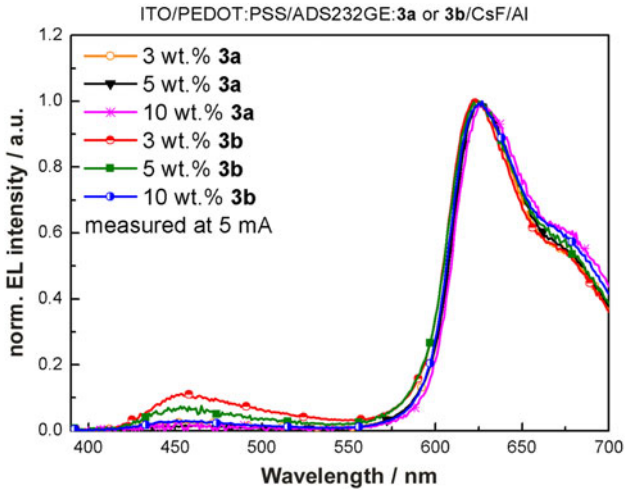

Fig. 11 Electroluminescence spectra of devices containing various amounts of **3a** or **3b** blended with ADS232GE as an active layer measured at 5 mA (device configuration: ITO/PEDOT:PSS/ADS232GE: **3a** or **3b**/CsF/Al)

loading could also be observed for these devices. Corresponding luminance values were 230 cd/m^2 (for 3 wt% of **3a**), 170 cd/m^2 (for 5 wt% of **3a**), and 90 cd/m^2 (for 10 wt% of **3a**) at 9 V (Fig. 10). Accordingly, devices prepared with **3a** showed lower luminescence values when compared with those prepared with **3b**. The same accounts for the current density. Nevertheless, energy transfer from the host polymer to the phosphorescent guest is more effective in the case of **3a**. While 10 wt% is needed to suppress the host emission in devices based on **3b**, 3 wt% of **3a** is sufficient to obtain electroluminescence spectra without a contribution from the host material.

Conclusion

Two platinum(II) quinolinolate complexes featuring different substitution patterns have been synthesized and characterized. The introduction of *tert*-butyl groups was initially done to reduce the tendency of such compounds to aggregate in solution, which is the main reason for the poor quantum yields obtained with this family of compounds. Results revealed that there is hardly any beneficial effect of the *tert*-butyl groups on characteristic photophysical properties like phosphorescent quantum yield or luminescent lifetime in solution. An examination of solid-state structures pointed in the same direction, since the packing of both compounds is characterized by π–π intermolecular interactions. Nevertheless, both complexes, regardless of their substitution pattern, are suited to use as emitter materials in OLEDs. Red to near-infrared electroluminescence with considerably low onset voltages (4–5 V) and cw luminance intensities exceeding 500 cd/m^2 were obtained using one of the complexes blended with a matching host material as the emissive layer of the device.

Experimental

Manipulations were performed under an inert atmosphere of purified nitrogen or argon using Schlenk techniques and/or a glovebox. Unless otherwise noted, materials were obtained from commercial sources (Aldrich, Fluka, or Lancaster) and were used without further purification. The solvents were purified according to standard procedures [53]. 3-(Hexyloxy)-2-phenylpyridine, 2-(4-*tert*-butylphenyl)pyridine, κ^2(N,C^2)-(2-(4-*tert*-butylphenyl)pyridine)-κ^1(N)-(2-(4-*tert*-butylphenyl)pyridine)chloroplatinum(II) (**1a**), κ^2(N,C^2)-(3-hexyloxy-2-phenylpyridine)-κ^1(N)-(3-hexyloxy-2-phenylpyridine)chloroplatinum(II) (**1b**) [38], (4-*tert*-butylphenyl)(8-hydroxyquinolin-5-yl)methanone (**2a**), and (8-hydroxyquinolin-5-yl)phenylmethanone (**2b**) [39] were prepared according to the literature.

NMR spectra were recorded on a Varian Inova 500 MHz spectrometer. Solvent residual peaks were used to reference the NMR spectra to the corresponding values given in the literature [54]. FT-IR spectra were obtained from films on KBr windows with a Perkin Elmer Spectrum One and a DTGS detector. UV–vis absorption spectra were recorded on a Cary 50 Bio UV–vis spectrophotometer, and fluorescence spectra on a Hitachi F-7000 fluorescence spectrometer equipped with an R928 red-sensitive photomultiplier from Hamamatsu. The emission spectra were not corrected for the sensitivity of the PMT. In order to measure the solid-state photoluminescence of complexes **3a** and **3b**, PMMA (polymethylmethacrylate) was mixed with 2 wt% of the complex and dissolved in 1 cm^3 of CH_2Cl_2.

Two hundred mm^3 of the blend mixture was drop-cast onto a glass slide and the solvent was evaporated. The films were measured at a 45° angle with respect to the incident light beam. Phase angle measurements in solution were performed using the following system. A dual-phase lock-in amplifier (DSP 830, Stanford Research Inc.) was used for sine-wave modulation of the LED at a frequency of 5.5 kHz and for detection. The optical system consisted of a blue LED ($\lambda_{max} = 470$ nm, Roithner Lasertechnik, Austria) combined with a BG 12 band-pass filter (Schott, Germany), and a red-sensitive PMT module (H5701-02, Hamamatsu, Germany) equipped with a long-pass filter (OG590, Schott, Germany). The measurements were carried out in aerated and in degassed $CHCl_3$ solutions. The apparent lifetimes were determined according to the equation $\tan\Delta\Phi = 2\pi\nu\tau$, where $\Delta\Phi$ indicates the phase shift, ν the modulation frequency and τ the luminescence lifetime. The relative quantum yield of luminescence was determined according Demas and Crosby [55] using 4-dicyanomethylene-2-methyl-6-(4-dimethylaminostyryl)-4H-pyrane ($\Phi = 0.57$) [44] as a standard. Combined differential scanning calorimetry (DSC)/thermogravimetric analysis (TGA) measurements were performed with a Polymer Laboratories STA 625 simultaneous thermal analyzer (crucibles: aluminum, from Rheometric Scientific). Thermal properties were determined in aluminum pans at a heat rate of 10 °C/min in a nitrogen flow of approximately 35 cm^3/min. MALDI-TOF mass spectra were recorded on a Micromass TofSpec 2E. The instrument was equipped with a nitrogen laser (337 nm wavelength, operated at a frequency of 5 Hz), and a time lag focusing unit. Spectra were taken in reflectron mode at an accelerating voltage of +20 kV. Analysis of data was done with MassLynx 3.4 (Micromass, Manchester, UK). Samples were dissolved in THF (1 mg/cm^3). Dithranol or retinoic acid was used as matrix (10 mg/cm^3 in THF). Solutions were mixed in the cap of a microtube in the ratio of 1 mm^3:10 mm^3. An amount of 0.5 mm^3 of the resulting mixture was spotted onto the target and air-dried. Electrochemical measurements were carried out with an Autolab PGSTAT100 high-voltage potentiostat/galvanostat (Eco Chemie B.V., Netherlands). For control, data acquisition, and analysis, the provided software—General Purpose Electrochemical System (GPES), version 4.9.004, developed by Eco Chemie—was used. The measurements were performed at a standard scan rate of 0.1 V/s in CH_2Cl_2/Bu_4BF_4 as electrolyte (0.1 M), using a three-electrode cell with a platinum disc electrode used as the working electrode, a platinum counter electrode, and a silver pseudo-reference electrode that was calibrated with ferrocene/ferrocenium as internal standard. Due to the poor conductivity of the solvent/supporting electrolyte, positive feedback IR compensation was used to eliminate the IR drop between the reference and working electrodes.

OLED fabrication was accomplished by the following procedures: poly[(9,9-dioctylfluorenyl-2,7-diyl)-co-(*N*,*N*′-diphenyl)-[*N*,*N*′-bis(*p*-butylphenyl)]-1,4-diaminobenzene] (ADS232GE) from American Dye Sources Inc. was used as the host polymer without further purification. The OLEDs consisted of a structured indium tin oxide (ITO) layer (from Balzers, 60 Ω m^{-2}), which was cleaned in an ultrasonic bath in toluene and isopropanol before an oxygen plasma cleaning step was performed. On the ITO electrode, a layer of poly(3,4-ethylenedioxythiophene)-polystyrenesulfonic acid (Baytron P VPAI 4083) from H.C. Starck was spin cast and subsequently dried under vacuum at 100 °C. The polymer layer was coated from a THF solution with a concentration of 6 g/dm^3 doped with 3, 5, and 10 wt% of **3a** and **3b**, respectively. This layer was subsequently dried for 1 h under dynamic vacuum at 100 °C. The evaporation of the top electrode took place at a base pressure of 1.1×10^{-6} mbar, and consisted of either a 10 nm calcium layer or a 1–3 nm CsF layer subsequently covered by 100 nm aluminum. The luminescence/voltage (LV) measurements were performed using an integrating sphere equipped with a silicon photodiode and a computer-controlled Keithley 237 source measurement unit. Spectral characterization was done with a LOT-ORIEL Multispec equipped with a DB 401-UV CCD camera from Andor.

$\kappa^2(N,C^2)$-(2-(4-tert-Butylphenyl)pyridine)-$\kappa^2(N,O)$-(5-(4-tert-butylphenyl)(8-quinolinolato-5-yl)-methanone)platinum(II) (**3a**, $C_{35}H_{34}N_2O_2Pt$)
Degassed CH_2Cl_2/EtOH = 1/1 (10 cm^3) was added to a mixture of **1a** (40.1 mg, 0.06 mmol), **2a** (28.16 mg, 0.09 mmol), and K_2CO_3 (42.5 mg, 0.31 mmol) contained in an oven-dried Schlenk tube. The reaction mixture was stirred at room temperature for 24 h. The solvent was then removed under reduced pressure, and the dried residue was suspended in CH_2Cl_2 and filtered over Na_2SO_4/Celite. Further purification was accomplished by column chromatography (neutral Al_2O_3, eluent: cy/ea = 5/1, $R_f = 0.35$ in CH_2Cl_2 on neutral Al_2O_3). Yield: 26.3 mg (60%); ^{1}H NMR (500 MHz, $CDCl_3$): $\delta = 9.58$ (d, 1H, $^3J = 8.5$ Hz, Q^4), 9.30 (d, 2H, $^3J = 5.1$ Hz, Py^6, Q^2), 7.88 (d, 1H, $^3J = 8.3$ Hz, Q^6), 7.82 (t, 1H, $^3J = 7.6$ Hz, Q^3), 7.73 (d, 2H, $^3J = 8.5$ Hz, $Ph^{2',6'}$), 7.64–7.59 (m, 3H, $Ph^{3,6}$, Py^4), 7.50 (d, 2H, $^3J = 8.3$ Hz, $Ph^{3',5'}$), 7.45 (d, 1H, $^3J = 8.1$ Hz, Py^3), 7.22 (d, 1H, $^3J = 8.1$ Hz, Ph^5), 7.15 (t, 1H, $^3J = 6.3$ Hz, Py^5), 6.96 (d, 1H, $^3J = 8.5$ Hz, Q^7), 1.44, 1.38 (s, 18H, $(CH_3)_3$) ppm; IR (film on KBr window cast from CH_2Cl_2 solution): $\bar{\nu} = 3{,}082$ (w), 3,030 (w), 2,958 (m), 2,927 (w), 2,905 (w), 2,862 (w), 1,634 (m), 1,608 (m), 1,590 (m), 1,578 (w), 1,563 (m), 1,503 (s),

1,466 (m), 1,436 (w), 1,389 (w), 1,364 (w), 1,340 (w), 1,312 (m), 1,272 (s), 1,204 (w), 1,190 (w), 1,163 (w), 1,150 (w), 1,105 (m), 1,077 (w), 1,067 (w), 1,041 (w), 1,015 (w), 908 (m), 852 (w), 823 (w), 779 (w), 769 (w), 753 (w), 720 (w), 712 (w) cm^{-1}; MALDI MS: $m/z = 708.2220$ (calcd 708.2247).

$\kappa^2(N,C^2)$-(3-Hexyloxy-2-phenylpyridine)-$\kappa^2(N,O)$-((8-quinolinolato-5-yl)phenylmethanone)platinum(II) (**3b**, $C_{33}H_{30}N_2O_3Pt$)

Degassed CH_2Cl_2/EtOH = 1/1 (10 cm^3) was added to a mixture of **1b** (100.7 mg, 0.136 mmol), **2b** (50.6 mg, 0.203 mmol), and K_2CO_3 (103.2 mg, 0.747 mmol) contained in an oven-dried Schlenk tube. The reaction mixture was stirred at room temperature for 24 h. The solvent was then removed under reduced pressure, and the dried residue was suspended in CH_2Cl_2 and filtered over Na_2SO_4/Celite. The solvent was removed and the orange residue was washed with 2 cm^3 MeOH to remove excess deprotonated 5-benzoyl-8-hydroxyquinoline. Further purification was accomplished by column chromatography (neutral Al_2O_3, eluent CH_2Cl_2, $R_f = 0.88$ in CH_2Cl_2 on neutral Al_2O_3). The solvent was removed and the dried residue was washed with 1 cm^3 MeOH and 5 cm^3 *n*-pentane and dried in vacuum, yielding an orange solid. Yield: 72.0 mg (76%) orange crystals; ^{1}H NMR (500 MHz, $CDCl_3$): $\delta = 9.61$ (d, 1H, $^3J = 8.5$ Hz, Q^4), 9.27 (d, 1H, $^3J = 5.1$ Hz, Q^2), 9.09 (d, 1H, $^3J = 5.6$ Hz, Py^6), 8.39 (d, 1H, $^3J = 7.8$ Hz, Ph^6), 7.85 (d, 1H, $^3J = 8.5$ Hz, Q^6), 7.77 (d, 2H, $^3J = 7.1$ Hz, $Ph^{2',6'}$), 7.64–7.61 (m, 1H, Q^3),7.58–7.47 (m, 4H, $Ph^{3',4',5'}$, Py^4), 7.39 (d, 1H, $^3J = 8.3$ Hz, Ph^3), 7.28–7.25 (m, 1H, Py^5), 7.16 (t, 1H, $^3J = 7.3$ Hz, Ph^5), 7.13–7.10 (m, 1H, Ph^4), 6.95 (d, 1H, $^3J = 8.5$ Hz, Q^7), 4.17 (t, 2H, $^3J = 6.3$ Hz, $OHex^1$), 1.99 (p, 2H, $OHex^2$), 1.60–1.56 (m, 4H, $OHex^{3,4}$), 1.43–1.37 (m, 2H, $OHex^5$), 0.94 (t, 3H, $^3J = 7.1$ Hz, $OHex^6$) ppm; $^{13}C\{^1H\}$ NMR (125 MHz, $CDCl_3$): $\delta = 195.8$ (1C, COPh), 172.3 (1C, Q^8), 156.6 (1C, Py^3), 153.3 (1C, Ph^2), 148.2 (1C, Py^6), 147.3, 147.2 (2C, Py^2, Q^{8a}), 141.7 (1C, Q^2), 140.8 (1C, Ph^1), 139.3 (1C, Ph^3), 138.9 (1C, $Ph^{1'}$), 138.6 (1C, Py^4), 131.9, 131.6, 131.5 (3C, $Ph^{4'}$, Q^4, Q^{4a}), 130.0 (2C, $Ph^{2',6'}$) 128.8, 128.7 (2C, Ph^6, Q^6), 128.3 (2C, $Ph^{3',5'}$), 123.7, 123.3 (2C, Q^3, Ph^5), 121.7, 121.6 (2C, Ph^4, Py^5), 118.4 (1C, Q^5), 113.9 (1C, Q^7), 69.5 (1C, $OHex^1$), 31.6 (1C, $OHex^4$), 29.1 (1C, $OHex^2$), 26.0 (1C, $OHex^3$), 22.7 (1C, $OHex^5$), 14.2 (1C, $OHex^6$) ppm; IR (film on KBr window cast from CH_2Cl_2 solution): $\tilde{\nu}$ = 3,093 (w), 3,044 (w), 2,929 (m), 2,857 (w), 1,629 (m), 1,572 (s), 1,558 (s), 1,503 (s), 1,468 (m), 1,427 (m), 1,389 (w), 1,365 (w), 1,341 (m), 1,310 (w), 1,272 (s), 1,213 (w), 1,199 (w), 1,144 (w), 1,111 (w), 1,060 (w), 1,024 (w), 899 (w), 823 (w), 794 (w), 782 (w), 752 (w), 730 (m), 708 (m) cm^{-1}; MALDI MS: $m/z = 696.1900$ (calcd 696.1884).

X-ray crystallography

Complexes **3a** and **3b** were crystallized by layering CH_2Cl_2 solutions of the respective complex with diethyl ether/pentane (**3a**) or diethyl ether (**3b**). In the case of **3b**, orange prisms of **3b**·1/2CH_2Cl_2 and orange needles of **3b**·3/2CH_2Cl_2 were obtained simultaneously. X-ray data of **3a**, **3b**·1/2CH_2Cl_2 and **3b**·3/2CH_2Cl_2 were collected on a Bruker Smart APEX CCD area detector diffractometer using graphite-monochromated Mo Kα radiation ($\lambda = 0.71073$ Å) and 0.3° ω-scan frames covering complete spheres of reciprocal space with $\theta_{max} = 30°$. After data integration with the program *SAINT+*, corrections for absorption, $\lambda/2$ effects, and crystal decay were applied with the program *SADABS* [56]. The structures were solved by direct methods (*SHELXS97*) and refined on F^2 with the program *SHELXL97* [57]. Non-hydrogen atoms were refined anisotropically. All H atoms were placed in calculated positions and thereafter treated as riding. The constraints $U_{iso}(H) = 1.2U_{eq}(C_{alkyl,aryl})$ and $U_{iso}(H) = 1.5U_{eq}(C_{methyl})$ were used. Selected crystallographic data are:

3a: $C_{35}H_{34}N_2O_2Pt$, $M_r = 709.73$, yellow plate, 0.39 × 0.25 × 0.05 mm, triclinic, space group *P*-1 (no. 2), $a = 6.3551(5)$ Å, $b = 14.4296(12)$ Å, $c = 15.5239(12)$ Å, $\alpha = 89.361(1)°$, $\beta = 82.535(1)°$, $\gamma = 84.146(1)°$, $V = 1404.1(2)$ Å^3, $Z = 2$, $\mu = 5.032$ mm^{-1}, $T = 100(2)$ K. 22,401 reflections were collected, corrected for absorption, and merged to 7,954 independent data ($R_{int} = 0.028$); final *R* indices: $R_1 = 0.0203$ [7,589 reflections with $I > 2\sigma(I)$], $wR_1 = 0.0537$ (all data), 367 parameters.

3b·1/2CH_2Cl_2: $C_{33}H_{30}N_2O_3Pt$·1/2CH_2Cl_2, $M_r = 740.14$, orange prism, 0.48 × 0.14 × 0.12 mm, triclinic, space group *P*-1 (no. 2), $a = 10.7057(6)$ Å, $b = 11.7931(7)$ Å, $c = 12.7720(7)$ Å, $\alpha = 103.710(1)°$, $\beta = 110.337(1)°$, $\gamma = 104.457(1)°$, $V = 1367.87(13)$ Å^3, $Z = 2$, $\mu = 5.266$ mm^{-1}, $T = 100(2)$ K. 25,234 reflections were collected, corrected for absorption, and merged to 7,913 independent data ($R_{int} = 0.026$); final *R* indices: $R_1 = 0.0210$ [7,502 reflections with $I > 2\sigma(I)$], $wR_1 = 0.0526$ (all data), 370 parameters. The dichloromethane molecule was found to be located about a symmetry center with consequent disorder of the CH_2 group.

3b·3/2CH_2Cl_2: $C_{33}H_{30}N_2O_3Pt$·3/2CH_2Cl_2, $M_r = 825.07$, orange needle, 0.59 × 0.07 × 0.06 mm, triclinic, space group *P*-1 (no. 2), $a = 8.2261(8)$ Å, $b = 13.7631(13)$ Å, $c = 15.2119(15)$ Å, $\alpha = 113.859(2)°$, $\beta = 94.726(2)°$, $\gamma = 98.024(2)°$, $V = 1541.2(3)$ Å^3, $Z = 2$, $\mu = 4.852$ mm^{-1}, $T = 100(2)$ K. 22,136 reflections were collected, corrected for absorption, and merged to 8,831 independent data ($R_{int} = 0.031$); final *R* indices: $R_1 = 0.0213$ [8,084 reflections with $I > 2\sigma(I)$], $wR_1 = 0.0494$ (all data), 402 parameters. One of the two crystallographically independent

dichloromethane molecules was found to be located about a symmetry center with consequent disorder of the CH_2 group. Compounds **3b**·1/2CH_2Cl_2 and **3b**·3/2CH_2Cl_2 differ significantly in the spatial arrangement of the Pt complexes and the conformation of the *n*-hexyl chains. CCDC 761429 (**3a**), 761430 (**3b**·1/2CH_2Cl_2), and 761431 (**3b**·3/2CH_2Cl_2) contain the supplementary crystallographic data for this paper. These data can be obtained free of charge from The Cambridge Crystallographic Data Center via http://www.ccdc.cam.ac.uk/data_request/cif.

Acknowledgments Financial support from the Austrian Science Fund (FWF) in the framework of the Austrian Nano Initiative (Research Project Cluster 0700—Integrated Organic Sensor and Optoelectronics Technologies—Research Project 0701 and 0715) is gratefully acknowledged. The authors thank Prof. Robert Saf and Karin Bartl for MALDI-TOF MS measurements and Gregor Trimmel for TGA data. Umicore's Precious Metals Chemistry division is acknowledged for a generous loan of K_2PtCl_4.

References

1. Thomas SW III, Yagi S, Swager TM (2005) J Mater Chem 15:2829
2. Kunugi Y, Mann KR, Miller LL, Exstrom CL (1998) J Am Chem Soc 120:589
3. Peyratout CS, Aldridge TK, Crites DK, McMillin DR (1995) Inorg Chem 34:4484
4. Koo C-K, Lam B, Leung S-K, Lam MH-W, Wong W-Y (2006) J Am Chem Soc 128:16434
5. Thomas SW III, Venkatesan K, Mueller P, Swager TM (2006) J Am Chem Soc 128:16641
6. Sax S, Fisslthaler E, Kappaun S, Konrad C, Slugovc C, Waich K, Mayr T, Klimant I, List EJW (2009) Adv Mater 21:3483
7. Stubenrauch K, Sandholzer M, Niedermair F, Waich K, Mayr T, Klimant I, Trimmel G, Slugovc C (2008) Eur Polym J 44:2558
8. Lu W, Mi BX, Chan MCW, Hui Z, Che CM, Zhu N, Lee ST (2004) J Am Chem Soc 126:4958
9. Ma B, Djurovich PI, Garon S, Alleyne B, Thompson ME (2006) Adv Funct Mater 16:2438
10. McGarrah JE, Eisenberg R (2003) Inorg Chem 42:4355
11. Wohlgenannt M, Tandon K, Mazumdar S, Ramasesha S, Vardeny ZV (2001) Nature 409:494
12. Miskowski VM, Houlding VH, Che CM, Wang Y (1993) Inorg Chem 32:2518
13. Aldridge TK, Stacy EM, McMillin DR (1994) Inorg Chem 33:722
14. Ionkin AS, Marshall WJ, Wang Y (2005) Organometallics 24:619
15. Berenguer JR, Lalinde E, Torroba J (2007) Inorg Chem 46: 9919
16. Hudson BP, Sou J, Berger DJ, McMillin DR (1992) J Am Chem Soc 114:8997
17. Ma B, Li J, Djurovich PI, Yousufuddin M, Bau R, Thompson ME (2005) J Am Chem Soc 127:28
18. Farley SJ, Rochester DL, Thompson AL, Howard JAK, Williams JAG (2005) Inorg Chem 44:9690
19. Yang C-J, Yi C, Xu M, Wang J-H, Liu Y-Z, Gao X-C (2006) Appl Phys Lett 89:233506
20. Xia H, Li M, Lu D, Zhang C, Xie W, Liu X, Yang B, Ma Y (2007) Adv Funct Mater 17:1757
21. Evans NR, Devi LS, Mak CSK, Watkins SE, Pascu SI, Koehler A, Friend RH, Williams CK, Holmes AB (2006) J Am Chem Soc 128:6647
22. Gong X, Lim SH, Ostrowski JC, Moses D, Bardeen CJ, Bazan GCJ (2004) Appl Phys 95:948
23. Wiesenhofer H, Zojer E, List EJW, Scherf U, Brédas JL, Beljonne D (2006) Adv Mat 18:310
24. Yersin H (2004) Triplet emitters for OLED applications. Mechanisms of exciton trapping and control of emission properties. In: Topics in current chemistry, vol 241. Springer, Berlin, pp 1
25. Van Dijken A, Perro A, Meulenkamp EA, Brunner K (2003) Org Electron 4:131
26. Tsuboyama A, Iwawaki H, Furugori M, Mukaide T, Kamatani J, Igawa S, Moriyama T, Miura S, Takiguchi T, Okada S, Hoshino M, Ueno K (2003) J Am Chem Soc 125:12971
27. Kappaun S, Rentenberger S, Pogantsch A, Zojer E, Mereiter K, Trimmel G, Saf R, Moeller KC, Stelzer F, Slugovc C (2006) Chem Mater 18:3539
28. Kappaun S, Sax S, Eder S, Moeller KC, Waich K, Niedermair F, Saf R, Mereiter K, Jacob J, Muellen K, List EJW, Slugovc C (2007) Chem Mater 19:1209
29. Kappaun S, Eder S, Mereiter K, List EJW, Slugovc C (2007) Eur J Inorg Chem 26:4207
30. Kappaun S, Slugovc C, List EJW (2008) Int J Mol Sci 9:1527
31. Niedermair F, Kwon O, Zojer K, Kappaun S, Trimmel G, Mereiter K, Slugovc C (2008) Dalton Trans 30:4006
32. Niedermair F, Sandholzer M, Kremser G, Slugovc C (2009) Organometallics 28:2888
33. Tang CW, VanSlyke SA (1987) Appl Phys Lett 51:913
34. Bergamini P, Bertolasi V, Ferretti V, Sostero S (1987) Inorg Chim Acta 126:151
35. Kato M, Ogawa Y, Kozakai M, Sugimoto Y (2002) Acta Crystallogr C58:m147
36. Yersin H (1997) Inorg Chem 36:3040
37. Shavaleev NM, Adams H, Best J, Edge R, Navaratnam S, Weinstein JA (2006) Inorg Chem 45:9410
38. Niedermair F, Waich K, Kappaun S, Mayr T, Trimmel G, Mereiter K, Slugovc C (2007) Inorg Chim Acta 360:2767
39. Matsamura K (1930) J Am Chem Soc 52:4433
40. Kim YH, Ahn JH, Shin DC, Kwon SK (2004) Polymer 45:2525
41. Ghedini M, Aiello I, La Deda M, Grisolia A (2003) Chem Commun 17:2198
42. Mdleleni MM, Bridgewater JS, Watts RJ, Ford PC (1995) Inorg Chem 34:2334
43. Kovelenov YA, Blake AJ, George MW, Matousek P, Mel'nikov MY, Parker AW, Sun XZ, Towrie M, Weinstein JA (2005) Dalton Trans 12:2092
44. Bondarev SL, Knyukshto VN, Stepuro VI, Stupak AP, Turban AA (2004) J Appl Spectrosc 71:194
45. Huber C, Klimant I, Krause C, Werner T, Mayr T, Wolfbeis OS (2000) J Fresenius Anal Chem 368:196
46. Lees AJ (1995) Commun Inorg Chem 17:319
47. Fernández S, Forniés J, Gil B, Gómez J, Lalinde E (2003) Dalton Trans 5:822
48. Pommerehne J, Vestweber H, Guss W, Mahrt RF, Baessler H, Porsch M, Daub J (1995) Adv Mater 7:551
49. Clark ML, Diring S, Retailleau P, McMillin DR, Ziessel R (2008) Chem Eur J 14:7168 (and references therein)
50. Piromreun P, Oh HS, Shen Y, Malliaras GG, Scott JC, Brock PJ (2000) Appl Phys Lett 77:2403
51. Greczynski G, Salaneck WR, Fahlman M (2001) Synth Met 121:1625

52. Williams JAG, Develay S, Rochester DL, Murphy L (2008) Coord Chem Rev 252:2596
53. Perrin DD, Armarego WLF (1988) In: Purification of laboratory chemicals, 3rd edn. Pergamon, New York
54. Gottlieb HE, Kotylar V, Nudelman A (1997) J Org Chem 62:7512
55. Demas JN, Crosby GA (1971) J Phys Chem 75:991
56. Bruker AXS Inc. (2003) Bruker programs: SMART (version 5.629), SAINT+ (version 6.45), SADABS (version 2.10), SHELXTL (version 6.14). Bruker AXS Inc., Madison
57. Sheldrick GM (1997) SHELX97: program system for crystal structure determination. University of Göttingen, Göttingen